

Aggregation Control of Squaraines and Their Use as Near-Infrared Fluorescent Sensors for Protein

Yongqian Xu,[†] Zhiyong Li,[‡] Andrey Malkovskiy,[§] Shiguo Sun,[‡] and Yi Pang*,[†]

Department of Chemistry & Maurice Morton Institute of Polymer Science and Department of Polymer Science, The University of Akron, Akron, Ohio 44325, and State Key Laboratory of Fine Chemicals, Dalian University of Technology, 158 Zhongshan Road, Dalian 116012, P. R. China

Received: April 1, 2010; Revised Manuscript Received: May 13, 2010

A series of squaraine dyes are found to be in H- or J-aggregates and are almost nonfluorescent in aqueous solution. Upon addition of bovine serum albumin (BSA), however, the fluorescence intensity ($\lambda_{\text{em}} \approx 690$ nm) increases by a factor of up to 200. Transformation of the dye molecules from the aggregates to the monomeric species appears to be responsible for the large fluorescence turn-on. While both H- and J-aggregates contribute to the observed fluorescence turn-on, the former appears to play a more important role. Electrophoresis imaging shows that these probes are good BSA indicators.

Introduction

Significant interest exists in developing fluorescent probes that can simply and quantitatively respond to individual proteins. The high sensitivity and selectivity of fluorescence probes offers a distinct advantage in the early diagnosis of diseases. Recently, several fluorescent reagents have been developed for the detection of proteins. However, some of the existing fluorescent reagents for protein detection suffer from the drawbacks of (1) long reaction time, (2) fluorescence turn-off, and (3) a nonlinear and sigmoidal calibration curve.^{1–3} Practical applications require the discovery of new systems that overcome these drawbacks.

Bovine serum albumin (BSA) is one of the most abundant proteins in blood plasma, which has been widely used as a model system to study protein folding, aggregation, and drug delivery. BSA plays a dominant role in the transport and deposition of endogenous and exogenous ligands in blood, since serum albumins often increase the apparent solubility of hydrophobic drugs in plasma and modulate their delivery to cells *in vivo* and *in vitro*.^{4–8} The specific delivery of ligands by serum albumins originates from the presence of two major and structurally selective binding sites, namely, site I and site II.^{4,8} The binding affinity of site I is mainly driven by hydrophobic interaction, while that of site II by a combination of hydrophobic, hydrogen-bonding, and electrostatic interactions. Probe design based on the different and novel interaction patterns could lead to useful tools for protein characterization.

For clinical applications, it is highly desirable to have fluorescent compounds that absorb and emit in the near-infrared region, since the problems of optical scattering, tissue absorbance, and autofluorescence are minimal in the NIR region.⁹ Squaraines (SQs) form a class of novel dyes which exhibit sharp and intense absorption and fluorescence in the red to near-infrared region. In solution, SQ dyes exhibit a high tendency to form J-aggregates that give red-shifted absorption bands (as compared to monomer absorption) or H-aggregates that give blue-shifted absorption bands. The different form of aggregates

also affects the emission properties, with H-aggregates usually being poor emitters and J-aggregates often giving efficient luminescence.^{10–12} Control of H- and J-aggregates in a polymethine dye can be achieved by forming an inclusion complex with a cucurbituril host.¹³ Proteins are biomacromolecules with hydrophobic pockets, whose binding to a suitable guest molecule could influence or disrupt the aggregates to turn on the fluorescence of SQs. Few studies have shown that SQ derivatives exhibit large fluorescence responses to BSA.^{14,15} Although the fluorescence response to BSA is assumed to be due to the reduced aggregation,¹⁵ more clear evidence is desirable to further understand the influence of protein binding on the aggregation. Among the H- or J-aggregates that a SQ dye can adopt, it is not clear how the different aggregate forms will affect the dye's fluorescence response to the protein species. The study is hampered by lack of the ability to tune the molecular structure toward H- or J-aggregation. In this study, we report a series of SQ 1, whose aggregate can be tuned (by the substituent R) to the H- or J-aggregates in aqueous solution (Figure 1). Evaluation of the SQ's response shows that the content of H- and J-aggregates can have significant impact on the dye's fluorescence turn-on response to BSA. Disruption of the aggregate structure is shown to be responsible for the dramatic fluorescence response (by over 200-fold), leading to a sensitive fluorescence turn-on probe for BSA detection in the near-infrared region (NIR, around 650–700 nm).

Experimental Methods

Reagents. All chemicals and reagents were used directly as obtained commercially unless otherwise noted. Water used was ultra filter deionized and purchased from Fisher Scientific. BSA ($\geq 98\%$), borax-boric acid, and sodium dodecyl sulfate (SDS, electrophoresis grade) were purchased from Acros Chemical; lysozyme, trypsin, and formaldehyde dehydrogenase were purchased from SIGMA. Thrombin was purchased from GE Healthcare.

Spectroscopic Measurements. NMR spectra were collected on a Varian 300 Gemini spectrometer. Mass spectrometric (MS) data were obtained on a HP1100LC/MSD mass spectrometer. High-resolution (HRMS) data were performed on a time-of-flight (TOF) MS system. UV-vis spectra were acquired on a

* To whom correspondence should be addressed. E-mail: yp5@uakron.edu.

[†] Department of Chemistry & Maurice Morton Institute of Polymer Science, The University of Akron.

[‡] Dalian University of Technology.

[§] Department of Polymer Science, The University of Akron.

Hewlett-Packard 8453 diode-array spectrometer. Fluorescence spectra were obtained on a HORIBA Jobin Yvon NanoLog spectrometer. The quantum yield of fluorescence of the sample was measured using bis(3-ethylbenzothiazol-2-ylidene)squaraine in ethanol ($\Phi = 0.21$) as a standard¹⁰ and calculated using eq 1:

$$\Phi_{\text{unk}} = \Phi_{\text{std}} \left(\frac{I_{\text{unk}}}{I_{\text{std}}} \right) \left(\frac{A_{\text{std}}}{A_{\text{unk}}} \right) \left(\frac{n_{\text{unk}}}{n_{\text{std}}} \right)^2 \quad (1)$$

where Φ_{unk} is the fluorescence quantum yield of the sample, Φ_{std} is the fluorescence quantum yield of the standard, I_{unk} and I_{std} are the integrated emission intensities of the sample and the standard, respectively, A_{unk} and A_{std} are the absorbance of the sample and the standard at the excitation wavelength, respectively, and n_{unk} and n_{std} are the refractive indexes of the corresponding solution.

General Procedure for the Sodium Dodecyl Sulfate Polyacrylamide Gel Electrophoresis (SDS-PAGE) and Gel Image. The electrophoresis experiment was carried out on a polyacrylamide mini gel (1 mm thick) using a discontinuous buffer system. The stacking gel contained 10% polyacrylamide in a 0.4 M borax-boric acid buffer solution (pH 8.7), and the separating gel contained 5% polyacrylamide in a 0.12 M tris-HCl buffer solution (pH 6.8). The running buffer contained 20 mM borax-boric acid, pH 8.7, and 0.1% (w/v) SDS in water. All solutions were freshly prepared prior to use. Sodium dodecyl sulfate polyacrylamide gel electrophoresis (SDS-PAGE) was carried out on a vertical polyacrylamide gel system until the protein bands reach the interface of the separating gel. Separation was performed at a constant voltage of 105 V. The instrumental setup consisted of an electrophoresis chamber (model DYCP-31DN) connected to a DYY-8C electrophoresis power supply, both from Beijing Liuyi Electrophoresis. The electropherograms were obtained on a Tanon GIS 2010 (Shanghai Tanon Sci. & Tec. Co., Ltd.) gel image system, and the data were analyzed by a Tanon image analysis software. The general staining procedure was as follows: Compound **1c** was dissolved in AcOH/MeOH/H₂O = 3:10:87 (v/v) at a concentration of 0.5 mg/mL with 0.5% (wt %) SDS. Bromophenol blue, which was added to the protein as an indicator, was washed off first, and the color changed from blue to shallow yellow after 2 h. The protein gels were stained with the solution of **1c** for 2 h, and images could be obtained using the image analysis system. Then the excess **1c** was removed from the gels by immersing the gels into the dye eluent and scanned using the image analysis system after 4 h.

Atomic Force Microscopy (AFM). Samples for the imaging were prepared by spin-casting the SQ dye solution (in H₂O containing 0.05 wt % SDS) in the absence and presence of BSA at the specified concentrations. AFM images were recorded under ambient conditions using a Park Scientific Autoprobe CP, which is operating in the tapping mode with Micromasch tapping probes with radius of curvature being <4 nm. The tips were brand new.

Results and Discussion

Synthesis and Characterization. The SQ dyes **1a–c** are synthesized by using a modified procedure reported previously (Figure 1).¹⁶ ¹H NMR of **1b** exhibits two vinyl signals at 6.55 and 6.18 ppm (1:1 ratio) (Figure 2), in contrast to one vinyl signal from **1c** at 6.0 ppm. Observation of two vinyl protons in **1b**, as well as two nonequivalent ethyl groups, indicates that the amino nitrogen has a strong interaction with the carbonyl group on the four membered SQ ring. The N–H proton of **1b**

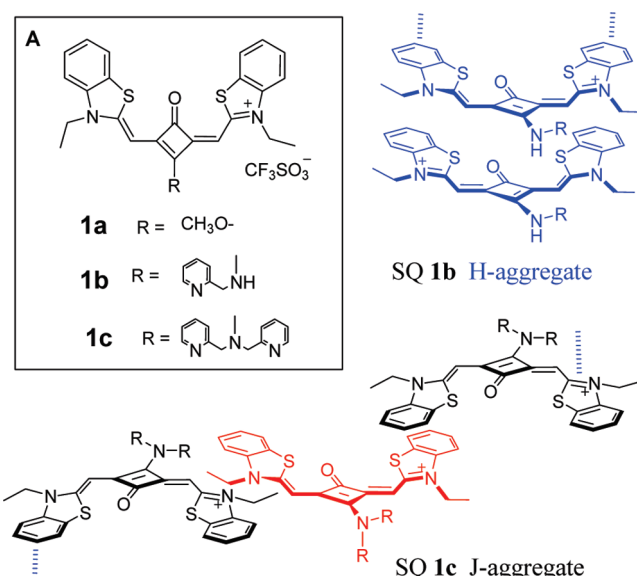


Figure 1. (A) Structure of the SQ dyes **1a–1c**. Postulated dye assemblies for an H-aggregate and a J-aggregate are shown outside panel A.

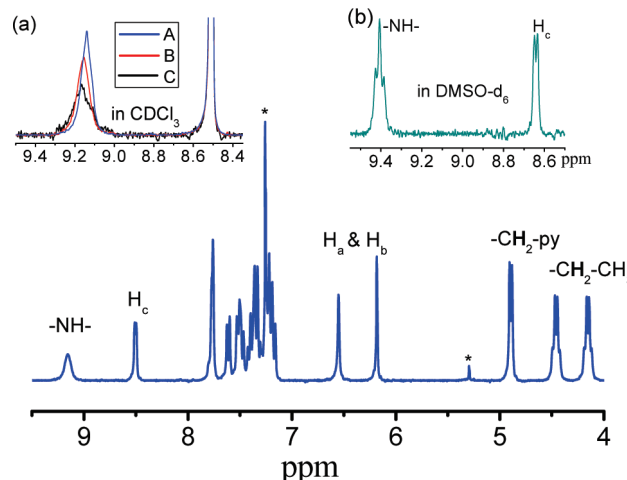


Figure 2. ¹H NMR spectrum of **1b** in CDCl_3 , where the starred (*) signals at 7.2 and 5.3 ppm are attributed to CHCl_3 and CH_2Cl_2 residue, respectively. The inset a shows the spectra of **1b** at different concentrations in CDCl_3 (solution concentration in the order: curve A > B > C). The inset b shows that the spectrum of **1b** in DMSO-d_6 .

in CDCl_3 occurs at 9.137 ppm as a broad peak (inset a, curve C). Further examination of the ¹H NMR spectrum of **1b** at diluted concentration shows that the resonance signal of N–H proton is slightly shifted downfield to 9.165 ppm (curve A). The trend suggests that the intermolecular hydrogen bonding is not likely to occur for **1b**, as weakening of the hydrogen-bonding by decreasing concentration would typically shifts the signal upfield.¹⁷ In the DMSO-d_6 solvent, the N–H signal of **1b** is shown as a relative sharp triplet ($\delta = 9.41$ ppm, $J = 6.3$ Hz) (Figure 2, inset b). In addition to the narrow signal, observation of the clear coupling between N–H and adjacent –CH₂– further supports the assumption that the N–H proton is reluctant to participate in the H-bonding with the nearby hydrogen bond acceptors such as DMSO.

UV-vis absorption spectra of **1** in various organic solvents give one band at about 670 nm with a similar absorbance, attributing it to the monomeric form (Figure 3 and S2, Table 1). Solvent polarity only slightly affects the absorption peak, with $\lambda_{\text{max}} = 676$ nm in the nonpolar toluene and $\lambda_{\text{max}} = 656$

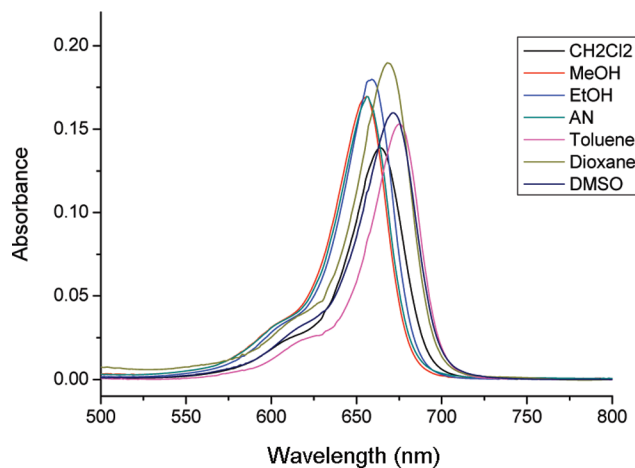


Figure 3. Absorption spectra of **1b** (5 μ M) in different solvents.

TABLE 1: Protein-to-Protein Variation of **1a–c**

proteins	1a	1b	1c
protein vs BSA			
BSA	1.00	1.00	1.00
lysozyme	0.14	0.37	0.19
trypsin	0.34	0.31	0.35
formaldehyde dehydrogenase	0.52	0.39	0.52
thrombin	0.06	0.03	0.19

nm in methanol for **1b**. Interestingly, the absorption spectrum of **1** in aqueous solution displays an additional peak that is about 50 nm blue-shifted from the monomer band (e.g., $\lambda_{\text{max}} = 591$ and 644 nm for **1b**), as a consequence of decreased solubility (Figure 4a). The new band at 591 nm can be assigned to H-aggregate on the basis of the observed spectral shift. The relative absorption intensity of the new bands falls in the order: **1b** > **1a** > **1c**, reflecting their relative tendency in forming the respective aggregate in aqueous solution. Addition of the anionic surfactant (SDS; 1.7 mM or 0.05 wt %), however, leads to strikingly different spectra (Figure 4b). For **1b** and **1c**, the new bands occur at longer wavelengths ($\lambda_{\text{max}} = 767$ and 757 nm, respectively), which are assigned to the J-aggregate. In sharp contrast, the new band for **1a** occurs at a much shorter wavelength ($\lambda_{\text{max}} = 470$ nm), whose narrow band characteristics suggest a well-defined structure. This high energy absorption

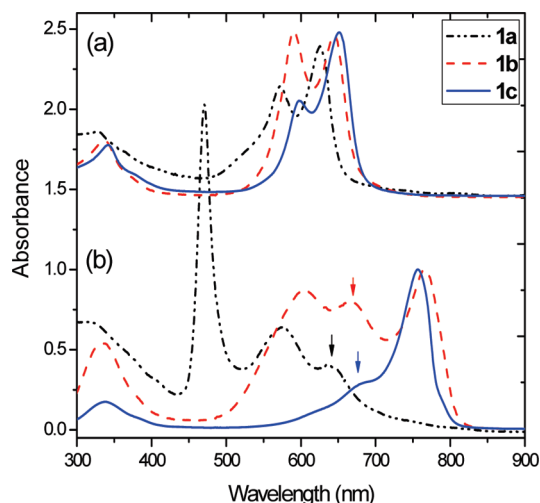


Figure 4. UV-vis absorption spectra of **1a–c** in water (5 μ M) in the absence (top) and presence (bottom) of 0.05% SDS. The arrows in the bottom panel indicate the corresponding monomeric species.

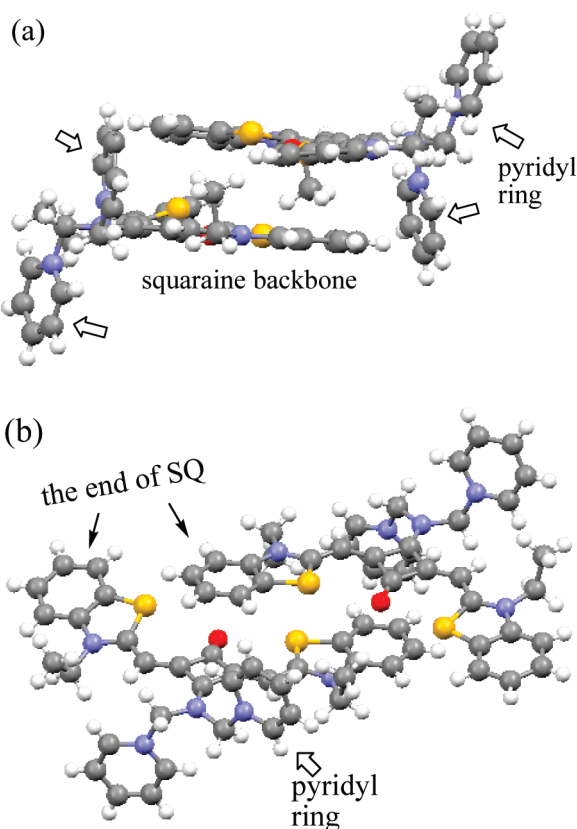


Figure 5. Crystal packing of **1c**. View a: two pyridyl groups are pointing toward opposite directions of the conjugated plane. View b: the tilted structure shows that one end of the SQ dye is aligned with the four-membered ring of the other SQ to give the arrangement like the J-aggregate assembly. In the structure, the carbon, oxygen, nitrogen, and sulfur atoms are in gray, red, blue, and yellow, respectively.

band is attributed to H-aggregate,^{18,19} since it is blue-shifted from the monomer absorption and not detected in other solvent systems. The finding clearly reveals that the interaction of SDS with the positive charge-bearing dyes **1** disrupts the noncovalent interactions between the dye molecules and promotes the J-aggregation for **1c** and H-aggregation for **1a**. Since the concentration of SDS is below its critical micelle concentration (cmc = 0.0082 M in pure water at 25 °C),²⁰ the surfactant molecules are expected to be in the single molecular form (not aggregate). It is possible that the anionic end of the surfactant interacts with the cationic site of **1**, thereby making the SQ dye less polar to promote the aggregation in aqueous solution. The reasons for the intriguing H- and J-aggregation selectivity are not fully understood.

Aggregation Structure. The steric bulkiness of the R group in **1** could play an important role in the H- or J-aggregation selectivity. On the basis of the crystal structural data,²¹ both sulfur atoms in **1** are on the same side as the oxygen of the four-membered ring. The two pyridyl groups in **1c** are pointing in the opposite direction of the SQ plane. Crystal packing of **1c** further reveals that the SQs are arranged in a manner similar to J-aggregate, in which the interacting SQs only overlap partially (i.e., one end of the SQ aligned with the four-membered ring of the other SQ) (Figure 5b). It can be assumed that the J-aggregate formed from **1c** in the aqueous solution adopts the similar arrangement.

The molecular arrangements in H- or J-aggregate are further examined by using molecular modeling (Figure 6). It should be noted that the H-aggregate formation requires the interacting chromophores to be parallel in close proximity, which is more

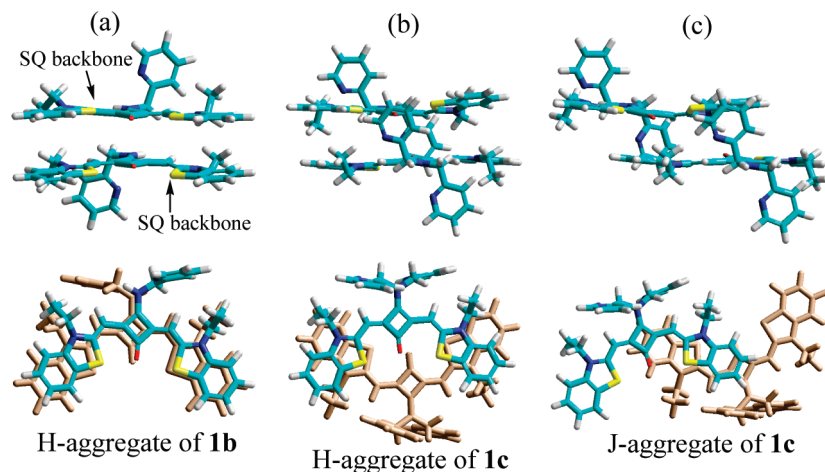


Figure 6. Molecular modeling of **1b** in H-aggregation (a) and **1c** in H-aggregation (b) and J-aggregation (c), which are viewed from the side (top row) and top (bottom row), respectively. In the top views (bottom row), one of the SQ dyes is shown in brown for clarity.

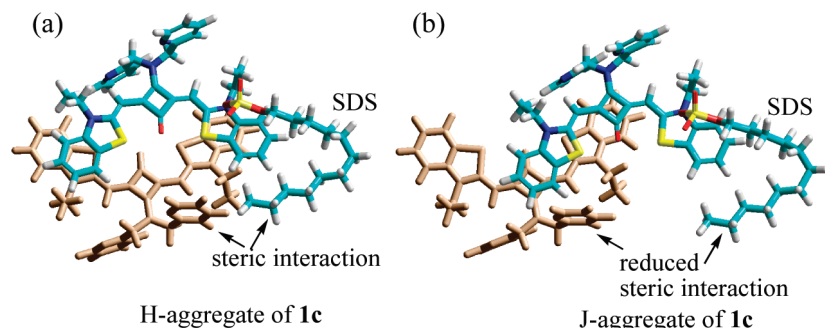


Figure 7. Schematic illustration of the interaction between the aggregate of **1c** and SDS. The steric interaction between the SDS chain and the pyridyl ring on the SQ backbone disfavors the H-aggregate (a), leading to the formation of the J-aggregate (b). For clarity, one of the SQs in the aggregate is shown in brown.

sensitive to the steric hindrance at the center of the chromophore (in comparison with J-aggregate). The SQ **1b** ($R = -\text{NH}-\text{CH}_2-\text{py}$) can adopt a parallel H-aggregate form (Figure 6a), in which the two molecules have a maximum $\pi-\pi$ interaction. Because of increased steric bulkiness ($R = -\text{N}-(\text{CH}_2-\text{py})_2$), the two SQ planes of **1c** in the H-aggregate are likely to have the antiparallel arrangement (Figure 6b), which is energetically less favorable because of the smaller overlap of conjugated backbones (smaller $\pi-\pi$ interaction). In other words, SQ **1c** has the least tendency to exhibit H-aggregate in aqueous solution (Figure 4a) and has a higher tendency to form J-aggregate. For the molecule **1a**, the smaller substituent ($R = -\text{OCH}_3$) increases its tendency to form parallel H-aggregate. In addition to the steric reasons, the impact for H- and J-aggregate formation appears to be dramatically enhanced by the addition of a small amount of SDS (Figure 4b), with **1a** giving primarily H-aggregate and **1c** forming mainly J-aggregate. The moderate steric bulkiness of $-\text{NH}-\text{CH}_2-\text{py}$ in **1b** could be responsible for the formation of both H- and J-aggregates. The role of possible hydrogen bonding with water molecules and SDS might be a less important factor for **1b** as indicated in the previous discussion (Figure 2). The influence of the added SDS can be rationalized by considering the steric interaction between the incoming SDS and SQs. Under the dilute conditions used, the alkyl chain of SDS in aqueous solution is likely to adopt a fold conformation in some degree to minimize its interaction with surrounding polar water molecules. When the SDS approaches **1c** in H-aggregate, the freely mobile alkyl chain could have some steric interaction with the pyridyl group (as shown in Figure 7a). This factor perturbs the H-aggregate structure to lead to energetically more favorable J-aggregate, in which the

pyridyl group is moved away from the SDS molecule (indicated by arrows in Figure 7b). In the SQ **1a**, such steric interaction with SDS is absent, and the association of SDS with **1a** reduces the solubility and promotes the H-aggregation of **1a**.

Absorption and Fluorescence Response to BSA. Absorption spectrum of **1b** in water reveals three peaks at 603, 670, and 766 nm (Figure 8a), which can be attributed to H-aggregate, monomer, and J-aggregate, respectively, on the basis of the observed spectral shift. Addition of BSA to the solution decreases the aggregation absorption bands at 603 and 766 nm, while the monomeric absorption band at 670 nm is notably increased. The result indicates that the BSA favors interaction with the SQ dye in the monomeric form. The same trend is also observed in the response of **1c** to BSA. Upon addition of BSA, the J-aggregate, which is observed as the predominant peak at $\lambda_{\text{max}} = 758$ nm in the UV-vis spectrum of **1c** (Figure 8b), gradually decreases along with increasing content for the monomeric species (minor peak at $\lambda_{\text{max}} = 677$ nm). Addition of the protein also caused the absorbance to increase at ≈ 270 nm, which corresponds to the tryptophan chromophore in BSA, suggesting that the interaction between SQs and tryptophan chromophore located at site I of BSA, mainly involving π -stacking and hydrophobic interaction.²² The analysis of absorbance data gave a 1:1 stoichiometry for the complexes between SQ dyes and BSA (Figure S4 of the Supporting Information, SI). The binding constants were calculated to be $5.0 \times 10^5 \text{ M}^{-1}$, $1.5 \times 10^6 \text{ M}^{-1}$, and $8.5 \times 10^5 \text{ M}^{-1}$ for **1a**, **1b**, and **1c**, respectively.

Compound **1** exhibits weak fluorescence in aqueous solution (**1a**: $\phi_f = 5.8 \times 10^{-3}$; **1b**: $\phi_f = 0.023$; **1c**: $\phi_f = 0.010$), due to its high tendency to form aggregates. In the presence of the

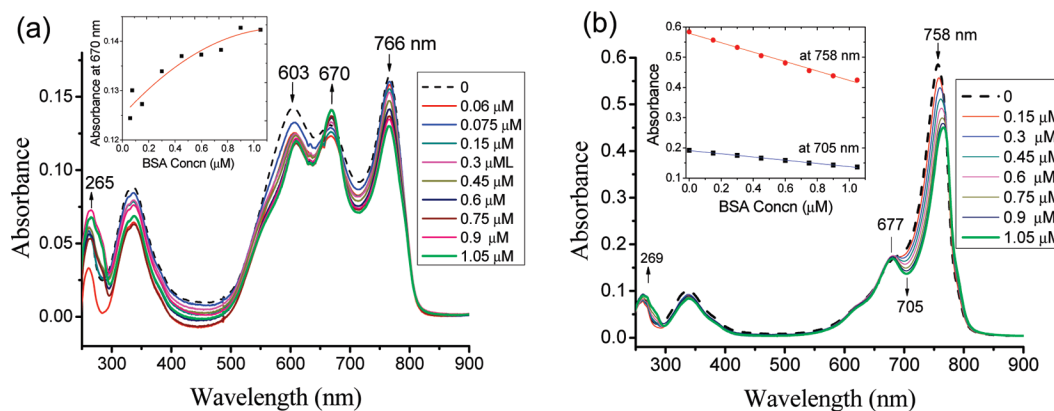


Figure 8. Absorption spectra of **1b** (a) and **1c** (5 μ M) (b) with different concentrations of BSA in water containing 0.05% SDS. The inset shows the absorbance response to protein concentration.

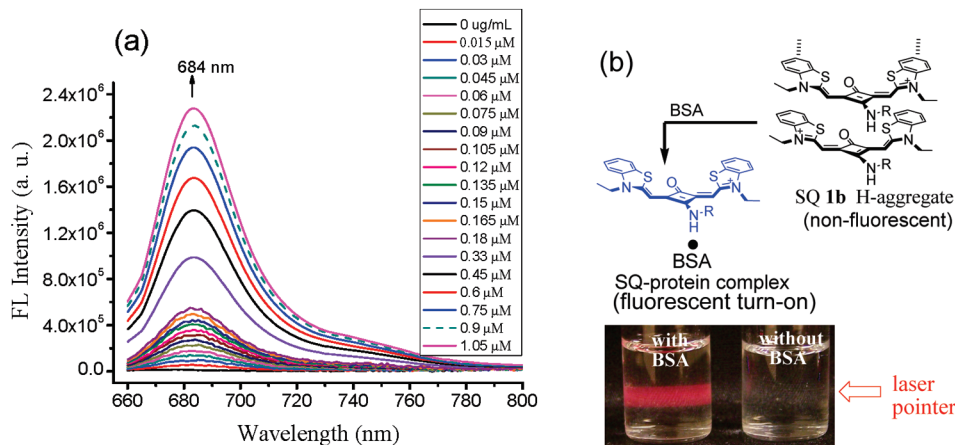


Figure 9. (a) Fluorescence spectra of **1b** (5 μ M) with different concentrations of BSA in water containing 0.05% SDS (excitation at 640 nm). (b) Photographs of **1b** solution in the presence and the absence of BSA, when the beam of a red laser pointer (wavelength: 630–680 nm) passes the solution from the right side.

anionic surfactant (SDS; 1.7 mM or 0.05 wt %), the fluorescence signals are further decreased by a factor of about 3 (Figure S5 and S6 of the SI). Interestingly, the fluorescence intensity (λ_{em} at \sim 690 nm) increases significantly upon addition of BSA (Figure 9). Although the J-aggregates have a strong absorption at \sim 760 nm, no fluorescence signals are detected near this wavelength, indicating that the J-aggregate from **1** is nonemissive. The emission signals at \sim 684 nm is assigned to the monomeric **1b**, as the fluorescence of SQ dye typically has a small Stokes shift (about 10–30 nm).^{10–12} The protein-induced fluorescence is visible by naked eye (Figure 9b), when a beam of regular laser pointer is passing the solution. Similar fluorescence enhancement is also observed from **1a** and **1c** after the addition of BSA (Figure S7 and S8 of the SI). In the presence of 70 mg/mL BSA and 0.05% SDS in aqueous solution, the quantum yields are determined to be $\phi_{\text{fl}} = 0.055$ for the **1a** + BSA, $\phi_{\text{fl}} = 0.31$ for **1b** + BSA, and $\phi_{\text{fl}} = 0.22$ for **1c** + BSA.

The intriguing BSA-induced fluorescence turn-on is attributed, at least in part, to the dissociation of SQ aggregates (which are nonfluorescent), as it is evident from the UV-vis absorption spectra (Figure 8). AFM (Figures 10 and S9 of SI) further confirms that the interaction with BSA strongly affects the aggregate. The aggregates of **1** are estimated to be in the range of 0.1–0.5 μ m (or 100–500 nm), which completely disappears in the presence of BSA (the size of the SQ-BSA complex is only about 20 nm). The results clearly point out that the fluorescence turn-on is due to the structural changes of aggregation, resulting from its interaction with proteins.

The fluorescence enhancement is dependent on the number of dye molecules which migrate from the aggregate states to the BSA binding sites (as nonaggregates). In responding to the BSA concentration, the fluorescence intensities of **1a**–**1c** exhibit a good linear correlation over a wide concentration range (up to \sim 0.45 μ M) (Figure 11). The fluorescence of **1b** is constantly higher than that of **1a** and **1c** in the BSA concentrations investigated, suggesting that the H-aggregates (poor emitter) of **1b** also play a positive role in the observed fluorescence turn-on. As seen from Figure 8a, the SQs of **1b** in both H- and J-aggregates are consumed about equally to interact with BSA. Higher fluorescence enhancement from **1a** than that from **1c** further suggests that the H-aggregate could contribute more to the enhancement than the J-aggregate. The assumption is consistent with the observation that the fluorescence enhancement from **1b** is approximately the sum of that from **1a** (primarily H-aggregate) and **1c** (primarily J-aggregate). The fluorescence enhancement upon binding BSA reaches over 200-fold, which is quite large in comparison with those being reported.^{3,15,23,24} The detection limit is 800 ng/mL of BSA (signal-to-noise ratio was 3).

A large fluorescence turn-on (\sim 200 fold), associated with the low conversion of “aggregate \rightarrow monomeric species” (Figure 8), suggests that the other factors may also be in play. Absorption spectra reveals that the SQs **1** are existing nearly exclusively in the *monomeric* form in ethanol (Figures S10 and S11 of the SI), attributed to its improved solubility. The fluorescence of the monomeric **1** is found to be increased significantly by the addition of glycerol, a viscous solvent which

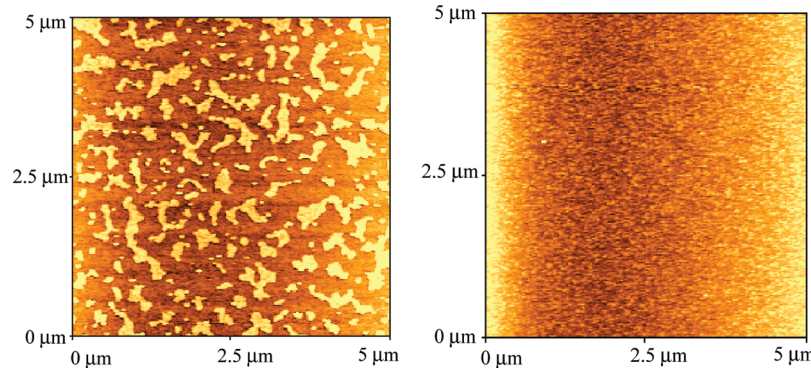


Figure 10. AFM images of **1c** (left) and BSA + **1c** (right) containing SDS (0.05 wt % in H_2O). The solution concentrations used for film preparation are 10 μM for the SQ dye and 23 $\mu\text{g}/\text{mL}$ (1.05 μM) for BSA.

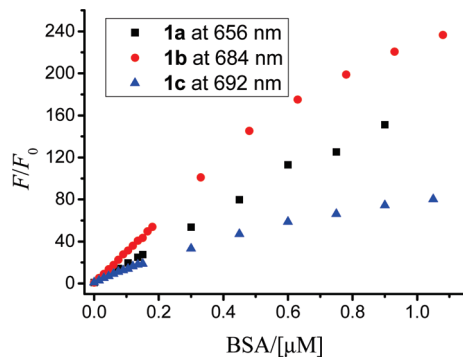


Figure 11. Plot of the fluorescence intensity of **1** as a function of BSA concentration. The plot uses the fluorescence intensities at the respective wavelengths (indicated in the inset).

is known to slow down the nonradiative decay rate (k_{nr}) of fluorescent molecules.²⁵ The result indicates that the fluorescence of the monomeric **1** can be significantly enhanced by changing the molecular environments. Therefore, it is likely that a tight binding to the protein environment, possibly at the hydrophobic pockets, increases the molecular rigidity of **1**, which reduces the vibrational modes and further raises the fluorescence signal.

The fluorescence response of **1a–c** to other proteins in aqueous solution in the presence of SDS (1.7 mM) are also investigated, and the results are summarized in Table 1. The response to BSA is normalized to 1.00. For other proteins, lysozyme, trypsin, formaldehyde dehydrogenase, and thrombin, the protein-to-BSA ratios are less than 0.52, showing that these SQ dyes exhibit some selectivity in responding to BSA. The observed selectivity can be attributed to the electrostatic interaction, because BSA is a negatively charged amphiphilic macromolecule,²⁶ which facilitates its interaction with the oppositely charged SQ dyes. In addition, BSA has hydrophobic pockets in its structure.^{27,28} These interactions serve as driving forces to transfer the dye molecules from their nonemissive aggregate states to the fluorescent monomeric form (via complexation with BSA). A lower response toward other proteins is presumably related to their different hydrophobic character, which is determined by the hydrophobicity of the constituent amino acids and the suitable hydrophobic “cleft” associated with the three-dimensional protein structures.²⁷

The response of **1c** to selective inorganic salts and reductants was examined to evaluate the interference. All of the tests were carried out by using 5 μM **1c** with one equivalent of BSA and 0.05 wt % SDS, in the presence of an excess amount of foreign substances. The maximum concentrations which perturb the fluorescence intensity by less than 10% are 1.0 mM for KNO_3 ,

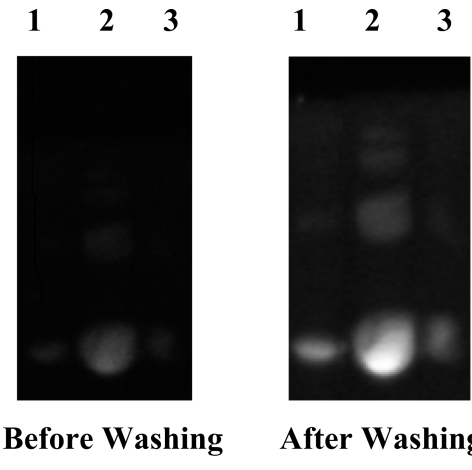


Figure 12. Fluorescence images of BSA stained by **1c** after electrophoresis. (1) BSA at 10 μg , (2) 110 μg , and (3) 2 μg before and after washing.

0.02 mM for ZnCl_2 and CaCl_2 , 0.1 mM for cyateine, and 0.02 mM for glutathione.

To illustrate the application of the BSA fluorescent indicator, BSA after electrophoresis using SDS-PAGE minigels were stained by **1c** and were scanned using image analysis systems. Figure 12 shows the images of BSA after staining with **1c**. The spots on the gels show that the SQ dye **1c** is sensitive for BSA sensing. The protein spot at 10 μg BSA after washing exhibited only slightly stronger fluorescence intensity than that at 2 μg . In comparison to the method of protein labeling reaction,²⁹ SQ dyes provide the noncovalent and special BSA sensing to avoid fussy and troublesome succinimidyl ester activated reaction of dyes before staining. SQ dyes, as a new kind of fluorogenic sensing that noncovalently binds to BSA, reveal great value for potential application.

Conclusion

In summary, we have demonstrated that SQ dyes **1a–c** have high tendency to form nonfluorescent H- and/or J-aggregates in aqueous solutions. With the aid of anionic surfactants, the SQ dyes can exist in primarily H-aggregate (for **1a**) or J-aggregate (for **1c**). Through noncovalent interaction with the biomacromolecules, these SQ dyes exhibit a large fluorescence response to proteins. The proposed fluorescence turn-on mechanism is based on the transformation of the dye molecules in aggregate states, which are nonfluorescent, to the fluorescent state upon protein binding. The H-aggregate appears to contribute more to the fluorescence enhancement. The rigid environment, achieved by strong complexation with protein, is

also believed to play an important role in the observed large fluorescence turn-on. The mechanism is consistent with the reasoning that the binding sites of proteins, which are located within the protein structure, favor the SQs in the monomeric rather than the more bulky aggregate forms on the basis of protein hydrophobicity. The new SQ probes have the following advantages: (1) a large fluorescence enhancement, reaching more than 200-fold upon binding BSA, (2) a fluorescence response in the NIR region ($\lambda_{\text{em}} \approx 690$ nm), and (3) a selective response to BSA over other proteins with low hydrophobic character.

Acknowledgment. This work was supported by The University of Akron and Coleman endowment. We are grateful for the protein samples provided by Dr. Weiping Zheng at University of Akron. We also wish to thank The National Science Foundation (CHE-9977144) for funds used to purchase the NMR instrument used in this work.

Supporting Information Available: Synthesis and experimental details and spectral characterization. This material is available free of charge via the Internet at <http://pubs.acs.org>.

References and Notes

- (1) Suzuki, Y.; Yokoyama, K. *J. Am. Chem. Soc.* **2005**, *127*, 17799–17802.
- (2) Suzuki, Y.; Yokoyama, K. *Angew. Chem., Int. Ed.* **2007**, *46*, 4097–4099.
- (3) Jisha, V. S.; Arun, K. T.; Hariharan, M.; Ramaiah, D. *J. Am. Chem. Soc.* **2006**, *128*, 6024–6025.
- (4) He, X. M.; Carter, D. C. *Nature* **1992**, *358*, 209–215.
- (5) Hirayama, K.; Akashi, S.; Furuya, M.; Fukuhara, K. *Biochem. Biophys. Res. Commun.* **1990**, *173*, 639.
- (6) Peters, T. J. *All about albumin: biochemistry, genetics, and medical applications*; Academic Press: San Diego, 1996.
- (7) Lu, J.; Stewart, A. J.; Sadler, P. J.; Pinheiro, T. J. T.; Blindauer, C. A. *Biochem. Soc. Trans.* **2008**, *36*, 1317–1321.
- (8) Dockal, M.; Carter, D. C.; Ruker, F. *J. Biol. Chem.* **1999**, *274*, 29303–29310.
- (9) Frangioni, J. V. *Curr. Opin. Chem. Biol.* **2003**, *7*, 626–634.
- (10) Das, S.; Thomas, K. G.; Ramanathan, R.; George, M. V.; Kamat, P. V. *J. Phys. Chem.* **1993**, *97*, 13625–13628.
- (11) Law, K. Y. *J. Phys. Chem.* **1987**, *91*, 5184–5193.
- (12) Law, K. Y. *J. Phys. Chem.* **1995**, *99*, 9818–9824.
- (13) Gadde, S.; Batchelor, E. K.; Weiss, J. P.; Ling, Y.; Kaifer, A. E. *J. Am. Chem. Soc.* **2008**, *130*, 17114–17119.
- (14) Volkova, K. D.; Kovalska, V. B.; Tatarets, A. L.; Patsenker, L. D.; Kryvorotenko, D. V.; Yamoluk, S. M. *Dyes Pigm.* **2007**, *72*, 285–292.
- (15) Wang, B.; Fan, J.; Sun, S.; Wang, L.; Song, B.; Peng, X. *Dyes Pigm.* **2010**, *85*, 43–50.
- (16) Santos, P.; Reis, L. V.; Duarte, I.; Serrano, J. P.; Almeida, P.; Oliveira, A.; Ferreira, L. F. V. *Helv. Chim. Acta* **2005**, *88*, 1135–1143.
- (17) Silverstein, R. M.; Webster, F. X.; Kiemle, D. J. *Spectrometric Identification of Organic Compounds*, 7th ed.; Wiley & Sons: New York, 2005; pp 150–154.
- (18) Khairutdinov, R. F.; Serpone, N. *J. Phys. Chem. B* **1997**, *101*, 2602–2610.
- (19) Barazzouk, S.; Lee, H.; Hotchandani, S.; Kamat, P. V. *J. Phys. Chem. B* **2000**, *104*, 3616–3623.
- (20) Mukerjee, P.; Mysels, K. J. *Critical Micelle Concentration of Aqueous Surfactant Systems*; U.S. National Bureau of Standards of NSRDS-NBS 36: Washington, DC, 1971.
- (21) Xu, Y.; Panzner, M.; Li, X.; Youngs, W.; Pang, Y. *Chem. Commun.* **2010**, *46*, 4073–4075.
- (22) Daban, J. R.; Bartolome, S.; Samso, M. *Anal. Biochem.* **1991**, *199*, 169–174.
- (23) Umezawa, K.; Citterio, D.; Suzuki, K. *Anal. Sci.* **2008**, *24*, 213–217.
- (24) Granzhan, A.; Ihmels, H. *Org. Lett.* **2005**, *7*, 5119–5122.
- (25) Peng, X.; Song, F.; Lu, E.; Wang, Y.; Zhou, W.; Fan, J.; Gao, Y. *J. Am. Chem. Soc.* **2005**, *127*, 4170–4171.
- (26) Peters, T. J. *Adv. Protein Chem.* **1985**, *37*, 161–245.
- (27) Matthews, B. W. Hydrophobic Interactions in Proteins. In *Handbook of Proteins: Structure, Function and Methods*; Cox, M. M., Phillips, G. N., Eds.; Wiley & Sons: New York, 2007; pp 45–50.
- (28) Gold, M. G.; Barford, D.; Komander, D. *Curr. Opin. Struct. Biol.* **2006**, *16*, 693–701.
- (29) Wang, D.; Fan, J.; Gao, X.; Wang, B.; Sun, S.; Peng, X. *J. Org. Chem.* **2009**, *74*, 7675–7683.

JP1029536